The potential of spectral and hyperspectral-imaging techniques for bacterial detection in food: a case study on lactic acid bacteria

Giorgia Foca[a], Carlotta Ferrari[a], Alessandro Ulrici[a], Giorgia Sciutto[b], Silvia Prati[b], Stefano Morandi[c], Milena Brasca[c], Paola Lavermicocca[d], Silvia Lanteri[e], Paolo Oliveri[e,*]

[a]*University of Modena and Reggio Emilia, Department of Life Sciences, Via Amendola 2, 42122 Reggio Emilia, Italy*
[b]*University of Bologna, Ravenna Campus, Microchemistry and Microscopy Art Diagnostic Laboratory (M2ADL), Via Guaccimanni 42, 48100 Ravenna, Italy*
[c]*National Research Council, Institute of Sciences of Food Production (CNR-ISPA), Via Celoria 2, 20133 Milano, Italy*
[d]*National Research Council, Institute of Sciences of Food Production (CNR-ISPA), Via Amendola 122/O, 70126 Bari, Italy*
[e]*University of Genova, Department of Pharmacy, Via Brigata Salerno 13, 16147 Genova, Italy*

*Corresponding author:
Paolo Oliveri Ph.D.
University of Genoa – Dept. of Pharmacy
Via Brigata Salerno, 13
I-16147 GENOA
Tel: +39 010 3532626
Fax: +39 010 3532684
e-mail: oliveri@dictfa.unige.it

Abstract

Official methods for the detection of bacteria are based on culture techniques. These methods have limitations such as time consumption, cost, detection limits and the impossibility to analyse a large number of samples. For these reasons, the development of rapid, low-cost and non-destructive analytical methods is a task of growing interest.

In the present study, the capability of spectral and hyperspectral techniques to detect bacterial surface contamination was investigated preliminarily on gel cultures, and subsequently on sliced cooked ham. In more detail, two species of lactic acid bacteria (LAB) were considered, namely *Lactobacillus curvatus* and *Lactobacillus sakei*, both of which are responsible for common alterations in sliced cooked ham.

Three techniques were investigated, with a different equipment, respectively: a macroscopic hyperspectral scanner operating in the NIR (10,470-5880 cm^{-1}) region, a FT-NIR spectrophotometer equipped with transmission arm as sampling tool, working in the 12,500-5800 cm^{-1} region, and a FT-MIR microscopy operating in the 4000-675 cm^{-1} region.

Multivariate exploratory data analysis, in particular principal component analysis (PCA), was applied in order to extract useful information from original data and from hyperspectrograms. The results obtained demonstrate that the spectroscopic and imaging techniques investigated can represent an effective and sensitive tool to detect surface bacterial contamination in samples and, in particular, to recognise the species to which the bacteria belong.

Keywords

FT-NIR spectroscopy; FT-IR microscopy; hyperspectral imaging; principal component analysis (PCA); lactic acid bacteria (LAB); cooked ham.

Highlights

- Official methods for detecting bacteria are culture-dependent
- Limitations of these methods are high time consumption, costs and detection limits
- Capability of sensitive spectral and hyperspectral techniques was investigated
- The potential of near and the infrared spectral regions were explored
- Multivariate exploratory data analysis was applied to extract useful information

1. Introduction

Food labelling regulations highlight the importance of providing the consumer with exact information about ingredients and additives present in food [1,2]. Such a key concern is reported also in the recent UE regulations, which applies from 2014 [3]. In particular, commission regulations also lay down microbiological criteria for foodstuffs, maximum limits for bacterial contamination, toxins and biogenic amines [4]. A direct consequence of this is the requirement for new analytical methodologies aimed at simplifying the use and improving the efficiency of existing control tools.

The shelf-life of cooked and sliced meat products, like cooked ham, is limited mainly because of microbiological safety and spoilage issues. This is because manipulations like slicing and packaging unavoidably reintroduce bacterial contaminants after the cooking process, and because the product has a near-neutral pH (around 6) and water activity higher than 0.945 [5,6].

Spoilage of packaged sliced ham is mostly accompanied by souring, slimy meat juice exudates and swelling of the pack due to gas production and is usually caused by lactic acid bacteria (LAB), together with *Pseudomonas*. Spoilage of cooked meat products results in sensory quality defects such as sour off-flavour, discolouration, gas production, and ropy slime formation.

Official methods for the detection of these bacterial species (ISO 15214:1998, ISO 13720:2010) are based on culture techniques. These methods have limitations such as time consumption, cost, detection limits and the impossibility to analyse a large number of samples. For these reasons, the development of rapid, low-cost and non-destructive analytical methods is a task of growing interest.

Methods based on classical spectroscopy and on the analysis of conventional images (RGB) have been studied extensively for several years [7]. Although applied to numerous food issues, these conventional approaches have a limited capacity for obtaining information from food samples, discarding either the spatial information – in the former approach – or the spectral one – in the latter [8]. In recent years, hyperspectral imaging (HSI) has emerged as a very efficient solution for the quality and safety control of food products, being able to thoroughly characterise individual components within complex matrices, allowing both chemical identification and localisation [9–13]. In fact, if the conventional image analysis gives an answer to the question 'where' and conventional spectroscopy may give answers to the two questions 'what' and 'how much', HSI gives an answer to the combined question 'where and how much of what', thus providing a comprehensive characterisation, particularly useful for identification and control purposes. In addition, collecting spectral profiles at multiple points in a given area increases the representativeness of the information obtained.

HSI can be used either on a macroscopic or a microscopic scale and in different spectral ranges, depending on the level of investigation and the spatial resolution required, the chemical information of interest to the particular issue and the type of implementation needed. The mid and near infrared regions are among the most useful from which to derive chemical information and to provide informative spectral fingerprints of the samples studied. In the case of food samples, for which colour is a basic quality characteristic to be assessed, also the visible region is often considerably informative.

HSI methods usually provide a considerable amount of data, structured in three dimensions (two spatial and one spectral) and are often highly complex, especially when working in the near infrared region, which is characterised by spectral overtone bands that often overlap considerably. In addition, the effective application of HSI techniques in routine food controls is currently limited by a series of problems, such as the presence of unwanted variations in the signals, due to factors beyond our control.

In order to minimise these problems and to extract information relevant for analytical purposes, it is essential to apply suitable signal processing and multivariate pattern recognition techniques [14].

In the last decades, great attention has been paid to the application of FT-IR spectroscopy in the field of microbial safety, thanks both to the ability of the technique to resolve complex mixtures in terms of composition and to the technological progress of modern instruments [15,16]. In particular, the coupling of microscopic devices and MIR spectroscopy offered significant advantages for the determination of compounds present at low concentration within heterogeneous matrices. Potential of FTIR techniques for identification of contaminant bacteria in food has been systematically investigated since the nineties of the 20th century, coupled with chemometric techniques, and proved to be able to perform not only species but also strain differentiations [17,18]. Recent studies efficiently coupled FTIR spectroscopy and microscopy for the characterisation of bacteria in fruit juices, dairy products and meat [19,20]. It is worth remarking that most of the approaches described in the literature include a separation step, aimed at extracting the bacterial cells from the complex food matrices before analysis. This compromises the advantages of low invasiveness towards sample and the performances of the method in terms of analysis time and cost.

In the present study, the capability of spectral and hyperspectral techniques to detect bacterial surface contamination was investigated preliminarily on gel cultures, and subsequently on sliced cooked ham. In more detail, two species of LAB were considered, namely *Lactobacillus curvatus* and *Lactobacillus sakei*, both of which are responsible for common alterations in sliced cooked ham.

LAB have been successfully studied by FTIR methods in the NIR and in the MIR spectral regions.

In particular, FTIR spectroscopy in the MIR range allowed the discrimination of the pure bacteria analysed in transmission mode [21]. In the present study, the potential of three techniques were investigated, with different equipment, respectively: a macroscopic hyperspectral scanner operating in the NIR (10,470-5880 cm^{-1}) region, a FT-NIR spectrophotometer equipped with transmission arm as sampling tool, working in the 12,500-5800 cm^{-1} region, and a FT-MIR microscopy operating in the 4000-675 cm^{-1} region.

Multivariate exploratory data analysis was applied in order to extract useful information from the data in order to verify the capability to distinguish the bacterial strains both in the culture and in the food matrix.

2. Materials and methods

2.1. Bacterial strains and culture conditions

The study was carried out using *L. curvatus* VZ22 and *L. sakei* VZ35 strains, isolated from Varzi PDO salami, and belonging to the bacterial collection of the Institute of Sciences of Food Production of the National Research Council of Italy (CNR-ISPA). The strains were identified by partial 16S rRNA sequencing according to McCabe and co-workers [22].

Before each experiment, the cultures were incubated overnight at 37 °C, in MRS broth (Scharlau Microbiology, Barcelona, Spain). *Lactobacillus* strains were streaked out in triplicate on MRS agar (Scharlau Microbiology), incubated at 37 °C for 72 h under anaerobic conditions (Anaerocult A, Merck Millipore, Darmstadt, Germany) and submitted to spectral and hyperspectral analysis.

Visual appearance of Petri dishes is shown in Figure S1 (Supplementary Material), with agar gel only (Figure S1.a) and with LAB cultures (Figures S1.b-c).

A commercial sliced cooked ham (about 2 mm thickness) was used for studying superficial contamination by the same LAB species and it was purchased from an Italian supermarket. The total load of bacteria of the slices before inoculum was < 10^3 cfu/g. A weighted amount (10 g) of sample was serially diluted in one-quarter-strength Ringer's solution and plated in Aerobic Count Plates (AC) Petrifilm (3M Canada, London, O Than, 1 mL of overnight cultures of *Lactobacillus* strains (about 10^8 cfu/mL) was centrifuged and washed twice with 1 mL of phosphate buffered saline (PBS), and then re-suspended in 1 mL of Ringer solution. Different spots within ham surface were artificially contaminated by deposition of 100 µL LAB suspensions (about 10^7 cfu/spot). After contamination, the solution was allowed to dry at room temperature and samples were immediately submitted to spectroscopic analyses.

2.2 Analytical techniques

2.2.1. FT-NIR spectroscopy

FT-NIR measurements were performed using a Bruker Optic MPA FT-NIR spectrophotometer equipped with transmission arm as sampling tool, working in the 12,500-5800 cm^{-1} region. The spectra were acquired in transmittance mode at 4 cm^{-1} resolution as the average of 32 scans. A rotating sample holder was used during spectra acquisition. This sampling procedure was necessary since the FT-NIR spectrophotometer used was not equipped with sampling tools suitable for punctual analysis. On the one hand, the rotation allows to eliminate the variation due to the intrinsic heterogeneity of the sample, on the other hand, the collected signal results in a sort of average of the characteristic signals of both LAB and agar gel. In fact, MRS agar was used as the chemical substrate on which bacteria were inoculated. In order to account for potential spectral interferences from the substrate, FT-NIR spectra were recorded both on the empty sample holder, as it is usually done in spectroscopy, and on the Petri dish containing the MRS agar substrate. In more detail, two series of spectra have been acquired on Petri dishes, considering two different backgrounds: an empty glass Petri dish (E series) and a polymeric (polypropylene) Petri dish containing the gel starter culture (G series). For each sample, two replicate measurements have been acquired for both the E and G series in two measurement sessions, following a different random sequence. The two different measurement sessions have been performed in the same day, by a time interval of less than one hour to evaluate measurement repeatability. As for the artificially contaminated cooked ham, the spectra were acquired under the same conditions used for Petri dishes, but the rotating sample holder was removed. In fact, in this case, the rotation of the sample would be inappropriate, since the contaminated area is located within a limited region of sample surface. An empty glass Petri dish was used for background measurement. Two replicate spectra were acquired for each sample in two measurement sessions, following a different random sequence.

2.2.2. NIR hyperspectral imaging

The hyperspectral imaging system consists of a desktop NIR Spectral Scanner (DV Optic) embedding a Specim N17E reflectance imaging spectrometer, coupled to a Xenics XEVA 2608 camera (320 x 256 pixels). The system covers the spectral range from 900 to 1700 nm (corresponding to 11110-5880 cm^{-1}) with a 5 nm resolution, for a total of 161 wavelengths.

Each image scene provided a data hypercube composed by 320 pixels per row and with a number of rows of 283 with a spatial resolution of 0.47 mm. A dark silicon carbide (SiC) sandpaper sheet was used as background for all the acquired images, since it is characterised by a very low and constant reflectance spectrum. In the image scene also different reference materials, i.e., a high-reflectance

white ceramic tile and two ceramic tiles with different grey-scale tones, have been included for the possible image correction, as already done in [23].

For each Petri dish, three replicate images have been collected in random order, in addition to four background measurements taken at different times during the acquisition session in order to better evaluate the stability of the system over time.

The same artificially contaminated cooked ham were imaged by simply placing the slice onto a sandpaper sheet. Two replicate images were acquired for each sample in two measurement sessions, following a different random sequence.

2.2.3. FT-MIR micro spectroscopy

A Thermo Nicolet (Thermo Fisher Scientific, Waltham, MA, USA), iN™10MX microscope, equipped with a mercury–cadmium–telluride detector cooled by liquid nitrogen, was used for spectroscopic analysis in the mid infrared region. The measurements were performed within the 4000-675 cm^{-1} region, at a spectral resolution of 4 cm^{-1}, spanning an area of 200x200 μm^2, by 128 scans.

In the case for LAB cultures on Petri dishes, reflection absorption spectroscopy (RAS) measurements on metallic substrate (gilded glass slides) were performed, at a 45° incidence angle [24]. Three micro samples were taken from each Petri dish and applied onto a gilded substrate, performing three replicate measurements were performed on each sample, thus recording a total number of 54 spectra.

In the case for artificially contaminated cooked ham, an attenuated total reflection (ATR) imaging system equipped with a conical germanium crystal and purchased by Thermo Fisher Scientific (Waltham, MA, USA) was applied for the characterisation of sample surfaces. In particular, three different slices of ham were contaminated with both of the two LAB. Measurements were performed after evaporation of the bacteria suspensions deposited. Several spectra were recorded on the contaminated and non-contaminated areas for each ham slice with an objective aperture of 400x400 μm^2 corresponding to an investigation area of about 100x100 μm^2.

A dedicated software, OMNIC Picta™ (Thermo Fisher Scientific, Waltham, MA, USA), was applied for a preliminary manipulation of spectral data.

2.3. Data processing and analysis

2.3.1. Exploratory analysis

Principal component analysis (PCA) was applied for exploratory purposes to the FT-NIR and to the FT-MIR datasets, separately. In particular, both of the FT-NIR data matrices – obtained by

considering the two different backgrounds – have size {16 × 1737}, while the FT-MIR data matrices have size {54 × 1725} (bacterial cultures on gel) and {746 × 1725} (bacteria on food matrix), respectively, where rows correspond to samples and columns correspond to the spectral variables recorded.

Several spectral pre-treatments, including Savitzki-Golay derivatives [25] and the standard normal variate (SNV) transform [26] were applied, both individually and in combination, in order to minimise unwanted signal variations, not related with chemical characterisation of bacterial samples.

As for the FT-NIR data, PCA was applied after column mean-centering, with the double aim of visualizing the data structure and detecting the presence of possible outliers (on the basis of the 99.7% confidence limit in the Q-T^2 plot).

In more detail, the detection of possible outliers is important since their presence can significantly affect the results of subsequent data analyses. In order to evaluate whether the samples identified as anomalous should be eliminated or are, instead, important to account for particular aspects of the system under study, two statistical parameters were considered: the distance of each sample from its projection on the hyperplane of the model, referred to as Q residual, and the distance of the projection of each sample on the PCA model from the centre of the model itself, referred to as Hotelling T^2.

Let $\mathbf{X}$ be a data matrix with size $\{n \times m\}$, obtained by measuring m variables on n samples. By means of PCA, the original data matrix $\mathbf{X}$ is decomposed into three matrices, the first one accounting for the variance associated to samples (score matrix, $\mathbf{T}$), the second one accounting for the variance associated to variables (loading matrix, $\mathbf{P}$) and the third one describing the non-systematic variation (residuals matrix, $\mathbf{E}$) according to the following equation:

$$\mathbf{X} = \mathbf{TP}' + \mathbf{E} = \sum_{a=1}^{A} \mathbf{t}_a \mathbf{p}_a + \mathbf{E} \quad (1)$$

Q residuals are calculated as the sum of squares of each row of the residuals matrix $\mathbf{E}$, according to the following equation for the i^{th} sample in $\mathbf{X}$, $\mathbf{x}_i$:

$$Q_i = \mathbf{e}_i \mathbf{e}_i' = \mathbf{x}_i (\mathbf{I} - \mathbf{PP}') \mathbf{x}_i' \quad (2)$$

where $\mathbf{e}_i$ is the i^{th} row of $\mathbf{E}$, $\mathbf{P}$ is the matrix of the A loading vectors considered in the PCA model and $\mathbf{I}$ is the identity matrix of appropriate size.

T^2 corresponds to the sum of normalised squared score values:

$$T_i^2 = \sum_{a=1}^{A} \frac{t_{ia}^2}{s_a^2} = \frac{t_{i1}^2}{s_1^2} + \frac{t_{i2}^2}{s_2^2} + \ldots + \frac{t_{iA}^2}{s_A^2} \quad (3)$$

where t_{ia} is the score value of the ith sample for the a^{th} PC and s_a^2 is the variance of the a^{th} score vector, $\mathbf{t}_a$, in the model.

By describing the unusual variation of each sample outside the model, high Q values indicate samples that do not follow the general pattern described by the PCA model. Conversely, the Hotelling T^2 parameter quantifies the samples variability within the model and the contribution of each sample in the definition of the model itself, so high T^2 values correspond to those samples which have mainly influenced the model.

2.3.2. Correction and segmentation of hyperspectral images

Intensity values of the raw images were converted into the corresponding reflectance values by applying a simple external calibration based on the high-reflectance standard reference and on the dark current measured by covering the camera lens with its cap [27]. Due to the low *S*/*N* ratio of spectra at the extremes of the measurement range, only the 150 spectral variables between 955 and 1700 nm (corresponding to 10470-5880 cm^{-1}) were considered for further analysis.

The first stage of the image processing (a preliminary exploratory data analysis step made by PCA on several merged images) evidenced that the acquisition system is very stable over time, therefore the images correction based on the reference materials included in the image scene was not necessary. In view of these results and in order to reduce the computational load, all the hyperspectral images were cropped, excluding the reference materials, to dimensions of 241 × 247 pixels.

PCA was then applied on each hyperspectral image, to segment the sample with respect to background pixels. To this aim, the effectiveness of several data pretreatments such as the standard normal variate (SNV) transform, detrending, first and second derivatives, column mean-centering and column autoscaling, were evaluated both separately and in different combinations.

2.3.3. Conversion of hyperspectral images into hyperspectrograms

The two datasets of segmented images, one for the Petri dishes and one for the ham samples, were converted into sets of one-dimensional signals, called hyperspectrograms, by means of a recently developed algorithm [28], which is derived from the colourgram approach, previously developed for the processing of RGB images [29–31].

This chemometric approach is aimed to significantly reduce the dataset size by compressing the useful information contained within each image into an artificial signal created by merging in sequence the frequency distribution curves of scores, Q residuals, Hotelling T^2 and loading vectors obtained by applying PCA on the single unfolded hypercube data. Hyperspectrograms can then be

used as a compact set of descriptors and submitted to further multivariate analysis techniques. This strategy also presents the great advantage of allowing for the simultaneous processing of tens up to hundreds of hyperspectral images.

The choice of the appropriate number of PCs to be retained in the PCA models used for the calculation of the hyperspectrograms does not represent a crucial point, since hyperspectrograms may be undergo a variable selection step, in which the PCs accounting for non-informative variability sources are discharged. In this case, a preliminary evaluation by PCA on a restricted number of representative images is performed, to provide an estimate of the number of PCs bringing useful information.

In Figure 1, the three average hyperspectrograms (corresponding to agar gel, *L. curvatus* and *L. sakei* classes) obtained from the Petri dish images are reported together with the description of the source of the various parts of the signals. In this case, a 5-PC model after column mean-centering as the pre-treatment was considered.

PCA was applied on the whole datasets of hyperspectrograms to detect the presence of possible outliers (the signals outside the 99.7% confidence limit in the Q-T^2 plot) and to visualise the data structure, as for common NIR spectra.

3. Results and discussion

3.1. FT-NIR spectra

Visual investigation of FT-NIR spectra acquired for the E and G series evidenced a slight but visible differentiation of the three classes of signals, in particular in the spectral region above 7500 cm^{-1}. The different series of spectra are reported in Figure S2 (Supplementary Material). It can be noticed that signals marked as the E series (empty sample holder as background) are more intense than those of the G series. For both of the series, signals corresponding to the three types of samples analysed are visually different, in particular at wavenumbers higher than 7500 cm^{-1}.

For both of the series of spectra, the PCA model obtained from the mean-centered data did not evidence the presence of outliers.

As for the E series, the PCA model (3 PCs, 97.7% explained variance) provided the PC1-PC2-PC3 score plot reported in Figure 2.a. In the 3-PCs space, the spectra corresponding to the *L. sakei* class form a cluster clearly distinguishable (in particular, along PC2) with respect to the others; the *L. curvatus* and the gel spectra are also distinguishable, though they appear quite close to each other; the third principal component evidently accounts for the different analytical sessions, which were separated by a time interval of less than one hour.

As for the G series, a 2-PC model was considered (96.6% explained variance). In Figure 2.b, the PC1-PC2 score plot is reported; the samples belonging to the three classes appear grouped into three distinct clusters. The cluster of *L. curvatus* appears more scattered in the PC space with respect to the *L. sakei* one. As explained in paragraph 2.2.1, FT-NIR spectra were acquired by averaging the signals collected during sample rotation. Looking at the corresponding RGB pictures in Figure S1 (Supplementary Material), it can be noticed that *L. curvatus* colonies seem to be less grown. This fact might be responsible for score distribution observed in the scatter plot: since *L. curvatus* colonies tended to occupy smaller areas on the agar surface, they may have contributed less to the average spectrum of each sample, which was also less repeatable. Comparing the models obtained for the two series of FT-NIR spectra, a 3D-score plot was helpful to efficiently distinguish signals belonging to the different types of samples for the E series, while a 2D-score plot was sufficient for the G series. Moreover, the percentages of variance explained by the three PCs in the case of the E series and by the two PCs in the case of the G series are very similar. These considerations indicate that use of MRS agar background over the empty sample holder for signal acquisition in future studies should be profitable.

Multivariate analysis of FT-NIR spectra recorded on cooked ham samples artificially contaminated with LAB did not allow to efficiently detect the presence of bacteria. PCA was applied using different spectra pre-treatments but, in each case, the three clusters corresponding to pure and contaminated ham (with *L. curvatus* and *L. sakei*, respectively) in the score plots were not distinguishable (*data not shown*).

This outcome could be due to different reasons, mainly concerning sensitivity of FT-NIR measurements, which is lower with respect to other spectroscopic techniques such as FT-MIR [32]. About this, Cámara-Martos and co-workers analysed in transmission different LAB water solutions in the 10^3-10^9 cfu/mL concentration range (the cell optical path used for the analysis of 1 mL of solution was not specified) [33]. They were able to distinguish the different bacteria in solutions containing high concentrations, but PCA was less effective for low concentrations.

In the present study, when 100 µL of LAB suspension having concentration of 10^8 cfu/mL were deposed over a flat surface, they were spread in a layer that is probably too thin (and so the LAB are too diluted) to be revealed. In addition, in the present work, the spectrum of samples was composed by the overlapping absorption bands of both ham and LAB but – at this level of dilution for the contaminants – the contribution of ham may be overwhelming.

In the literature, a number of works about the assessment of microbial contamination of flesh by using NIR-based methods, in particular hyperspectral imaging, can be found. In almost all of these works, the amount of bacteria is estimated in meat and fish samples stored under controlled

conditions for different time intervals, ranging from a few hours to several days: under these conditions, samples undergo bacterial spoilage. Such a spoilage, which is responsible for off-flavours and slime formation, becomes apparent when microorganisms have reached concentrations around 10^7-10^8 CFU/g, depending on muscle type and pH [34]. At this point, food is definitely decayed from a sensory point of view and should be considered unsafe for human consumption.

Concerning the use of classical FT-NIR spectroscopy, Lin and co-workers [35] applied short-wavelength near-infrared diffuse reflectance spectroscopy in the 600–1100 nm region to quantify microbial loads in chicken meat. Although they achieved satisfactory results, they remarked that sample spoilage produces biochemical changes in chicken meat (mainly proteolysis, indicated by the release of free amino acids), so that NIR measurements revealed the extent of biochemical changes in chicken – correlated to microbial spoilage – rather than directly measuring the presence of bacteria on breast muscle surface.

3.2. NIR hyperspectral images

Among the combinations of pre-treatments evaluated, detrending combined with column mean-centering provided the best distinction of the pixel cluster corresponding to the Petri dish from the clusters formed by background pixels. The score images obtained for all the sample images evidenced that the second PC allowed a clear distinction between the Petri dish and the background. In more detail, a threshold value of PC2 score equal to 0 was found to be useful to remove the background and the Petri dish border. As the final step, a further control aimed at manually removing extraneous pixels eventually not excluded was performed. As an example, the image of a *L. curvatus* sample, before and after segmentation, is reported in Figure 3.

A PCA model obtained on the hyperspectrogram dataset considering a number of significant PCs equal to 3 (accounting for about 65% of the total variance) did not reveal outliers. Looking at the PC1-PC2 score plot (Figure 4), three clusters corresponding to the three different classes were distinguished; in particular, PC1 allowed a clear separation of gel from bacteria samples, while PC2 allowed to distinguish between the two different bacterial species. Since the hyperspectrogram approach allows to condense the information of a whole image into a single signal, it can be used to estimate the actual repeatability of replicate images. In Figure 4, the replicates of the same samples were indicated by using the same symbol, and this allowed to verify, with few exceptions, the reproducibility of the system. This finding suggests that performing PCA on hyperspectrograms could be also considered a valuable alternative method to evaluate the instrumental stability over time, for instance using standard images, or to investigate a dynamic process such as sample ageing.

Also in this case, analysis of hyperspectrograms obtained from the segmented images acquired on artificially contaminated ham did not evidenced neither the presence nor the type of bacteria (*data not shown*). The possible reasons for this failure are similar to those invoked in the case of FT-NIR spectra: absorption bands of ham may be overwhelming with respect to the LAB ones, and the concentration of bacteria over the ham surface is too low to be revealed. In addition, instrumentation for the acquisition of hyperspectral images does not explore the entire NIR spectral range.

Very recent research works proved that imaging techniques would allow to estimate the extent of bacterial contamination on meat and fish samples. As an example, He et al. [36] assessed LAB values in salmon fillets during a 12-day cold spoilage process. Their study confirmed that no typical absorption band of LAB was found in the spectral profiles, but spectral data of salmon samples could be mined – by using suitable chemometric tools – to indirectly predict LAB, as the growth of LAB is closely related with chemical composition of salmon flesh. In the work by Tao et al. [37], a particular hyperspectral imaging system was used, namely the hyperspectral scattering system, in which point light is applied as the illuminant source, in a manner that the backscattering image of samples is captured. During the meat spoilage process, meat microstructure undergoes changes, together with bacterial load and chemical composition. These changes could be reflected by the derived light absorption and scattering features from the hyperspectral scattering image. Barbin and co-workers [38] investigated by HSI the microbial growth in pork meat samples stored under refrigerated conditions during 21 days. They were able to classify samples as fresh or spoiled, and the comparison of the spectral features of the two sample categories allowed to determine how microbial spoilage affects spectral fingerprints of pork meat. The main differences were observed in the wavelength range between 1300 nm and 1600 nm, where N–H stretching of proteins (amines and amides) and their interactions with water are observed: this suggests the occurrence of proteolytic changes, which are recognised as the main indicator for the starting of spoilage in meat products.

Concerning the study of bacterial surface contamination of sliced cooked ham, the focus of the present study was on early detection of LAB presence before ham undergoes evident chemical and physical changes: for this reason, samples were analysed just after evaporation of LAB suspensions deposited. Therefore, the failure of NIR-based methods to evidence the presence of LAB on ham surface are potentially due to the lack of spoilage of the matrix, which is – conversely – a key aspect in all of the studies mentioned above.

448 *3.3. FT-MIR micro spectroscopy*

449 FTIR microscopy in the MIR region presents the disadvantage of requiring an appropriate sampling
450 both of the bacterial cultures and of the food matrix contaminated with bacteria. However, working
451 at the microscopic scale, it is possible to obtain spectra related to small area thus allowing to
452 maximise the signal of bacteria, with respect to that of the matrix, in the points in which they are
453 present. Accordingly to what was observed by Oust and co-workers [21], Figure S2 (Supplementary
454 Material) shows the average profile of FT-MIR RAS spectra recorded for *L. curvatus* (FigureS2.a)
455 and *L sakei* (Figure S2.b) from gel cultures, respectively. The main bands are ascribable to amide
456 N-H stretching (3200 cm^{-1}), amide I and II bands (near 1650 cm^{-1} and 1540 cm^{-1}, respectively),
457 related to the protein pattern [39], and to C=O stretching of lipid esters (shoulder visible at 1743
458 cm^{-1} in Figure S2.b) [19]. As a matter of facts, the whole protein pattern has been reported as a key
459 difference between the two species [40,41].

460 PCA applied to the whole dataset (27 spectra recorded for each bacterial species) shows that the
461 MIR spectra recorded contain information useful to identify the two *Lactobacillus* species.

462 In particular, Figure 5.a reports the PC1-PC3 score plot obtained after application of SNV
463 transform, first derivative and column mean-centering. Two well defined clusters, corresponding to
464 *L. sakei* (blue) and *L. curvatus* (red), respectively, are evident, even though an important dispersion
465 among analytical replicates is noticeable. Figure 5.b show the corresponding loading plot, in which
466 it is possible to identify spectral variables around 1620-1650 cm^{-1} (amide I band) and 1740 cm^{-1}
467 (ester band) as the most involved in the characterisation of the two bacterial species.

468 Analysis of FT-MIR reflection spectra recorded on cooked ham samples artificially contaminated
469 with LAB showed that signals in the mid-infrared region are useful to detect and identify bacterial
470 species also on the surface of real food matrices.

471 Outcomes of PCA, after application of SNV transform, second derivative and column mean-
472 centering, are shown in Figure 6. The PC1-PC2 score plot (Figure 6.a) clearly shows a
473 differentiation between non-contaminated areas (blue scores) and portions of ham surface
474 contaminated with *L. curvatus* (red scores) and *L. sakei* (green scores), respectively.

475 From a joint analysis of the corresponding loading plot (Figure 6.b), the main role of ester and
476 amide bands (at around 1740 and 1620 cm^{-1}, respectively) for the characterisation of bacteria is
477 confirmed. Simultaneously, a band around 2916 cm^{-1}, ascribable to C-H stretching emerges as a
478 marker for the differentiation of the two LAB species on ham

479

480 **4. Conclusions**

The results obtained in this study demonstrate that the spectroscopic techniques investigated may represent an effective screening tool to detect surface bacterial contamination in samples and, in particular, to recognise the species to which bacteria belong. All the techniques applied proved to be effective when LAB are laid down on a simple matrix, such as MRS agar. Concerning the Petri dish samples, both FT-NIR and FT-MIR techniques gave very satisfactory results on spectra treated using common signal pre-processing methods. In the case of hyperspectral images, the datacubes were converted into hyperspectrograms before performing exploratory analysis by PCA. Conversion of images into hyperspectrograms is appropriate, as demonstrated by the encouraging results obtained. In particular, this novel approach has proved to be effective to extract the useful information from the images and, at the same time, to disregard the uninformative one.

When LAB are inoculated on a more complex matrix, such as sliced cooked ham, not all of the spectroscopic techniques worked equally well. Preliminary tests indicated that FT-MIR microscopy may provide satisfactory responses when dealing with real food samples contaminated at spoilage concentration, also thanks to the fact that it allows localised investigations to be performed. On the contrary, neither FT-NIR nor NIR hyperspectral imaging were effective in detecting the presence and the type of bacteria. The main reason for these outcomes may be ascribable to the limited sensitivity of NIR-based spectroscopic techniques with respect to FT-MIR.

These preliminary results suggest that a more in-depth investigation is required, which could be interesting because NIR-based techniques have many advantages in terms of practical applications and implementation of routine control systems. In particular, FT-NIR measurements are very fast – though not so sensitive – so they could be used for screening purposes; when the spectrophotometer is equipped with fiber optic probes, also online screening is possible. Further advantages connected to NIR imaging implementations involve the possibility to visualise the location of contaminated areas on the sample. The hyperspectrogram approach, in which each image is converted into a signal, still allows the spatial localisation of the contamination through the reconstruction of false color images after multivariate data analysis [42]. In addition, the conversion of each image into a signal of few hundreds of points enables the simultaneous modelling of tens (but it also works for hundreds) of hyperspectral images. In this way, NIR imaging might be implemented as a suitable system for monitoring different species of bacterial contaminants directly in industrial plants.

FTIR microscopy in the MIR region seems a promising tool for the identification of contaminated food matrix. However, being a micro chemical technique just a small area at a time can be analysed, and a proper sampling strategy is needed. Thus, this approach may find application to confirm or refine preliminary screening data obtained with macro techniques such as FT-NIR and NIR hyperspectral analyses.

References

[1] CE Regulation n. 1333/2008.

[2] DL 109/1992.

[3] CE Regulation n. 1169/2011.

[4] CE Regulation n. 1441/2007.

[5] P. Hu, G. Zhou, X. Xu, C. Li, Y. Han, Characterization of the predominant spoilage bacteria in sliced vacuum-packed cooked ham based on 16S rDNA-DGGE, Food Control. 20 (2009) 99–104. doi:10.1016/j.foodcont.2008.02.007.

[6] C. Cantoni, S. Milesi, L. Iacumin, Bacterial alterations of cooked packaged hams and the responsibility of Enterococcus faecalis in these defect, Ind. Aliment. 48 (2009) 31–35.

[7] A. Gowen, C. O'Donnell, P. Cullen, G. Downey, J. Frias, Hyperspectral imaging – an emerging process analytical tool for food quality and safety control, Trends Food Sci. Technol. 18 (2007) 590–598. doi:10.1016/j.tifs.2007.06.001.

[8] H. Cen, Y. He, Theory and application of near infrared reflectance spectroscopy in determination of food quality, Trends Food Sci. Technol. 18 (2007) 72–83. doi:10.1016/j.tifs.2006.09.003.

[9] I. Kavdir, R. Lu, D. Ariana, M. Ngouajio, Visible and near-infrared spectroscopy for nondestructive quality assessment of pickling cucumbers, Postharvest Biol. Technol. 44 (2007) 165–174. doi:10.1016/j.postharvbio.2006.09.002.

[10] D.W. Sun, Hyperspectral Imaging for Food Quality Analysis and Control, Elsevier Inc., 2010.

[11] J.M. Amigo, H. Babamoradi, S. Elcoroaristizabal, Hyperspectral image analysis. A tutorial, Anal. Chim. Acta. 896 (2015) 34–51. doi:10.1016/j.aca.2015.09.030.

[12] J.M. Amigo, Practical issues of hyperspectral imaging analysis of solid dosage forms., Anal. Bioanal. Chem. 398 (2010) 93–109. doi:10.1007/s00216-010-3828-z.

[13] C. Esquerre, A. Gowen, G. Downey, C. O'Donnell, Wavelength selection for development of a near infrared imaging system for early detection of bruise damage in mushrooms (Agaricus bisporus), J. Near Infrared Spectrosc. 20 (2012) 537. doi:10.1255/jnirs.1014.

[14] J. Burger, A. Gowen, Data handling in hyperspectral image analysis, Chemom. Intell. Lab. Syst. 108 (2011) 13–22. doi:10.1016/j.chemolab.2011.04.001.

[15] D. Alexandrakis, G. Downey, A.G.M. Scannell, Rapid Non-destructive Detection of Spoilage of Intact Chicken Breast Muscle Using Near-infrared and Fourier Transform Mid-infrared Spectroscopy and Multivariate Statistics, Food Bioprocess Technol. 5 (2009) 338–347. doi:10.1007/s11947-009-0298-4.

[16] F. Valerio, P. De Bellis, M. Di Biase, S.L. Lonigro, B. Giussani, A. Visconti, et al., Diversity of spore-forming bacteria and identification of Bacillus amyloliquefaciens as a species frequently associated with the ropy spoilage of bread., Int. J. Food Microbiol. 156 (2012) 278–85. doi:10.1016/j.ijfoodmicro.2012.04.005.

[17] D. Naumann, V. Fijala, H. Labischinski, The differentiation and identification of pathogenic bacteria using FT-IR and multivariate statistical analysis, Mikrochim. Acta. 94 (1988) 373–377. doi:10.1007/BF01205910.

[18] D. Naumann, D. Helm, H. Labischinski, Microbiological characterizations by FT-IR spectroscopy., Nature. 351 (1991) 81–2. doi:10.1038/351081a0.

[19] R. Davis, J. Irudayaraj, B.L. Reuhs, L.J. Mauer, Detection of E. coli O157:H7 from ground beef using Fourier transform infrared (FT-IR) spectroscopy and chemometrics., J. Food Sci. 75 (2010) M340–6. doi:10.1111/j.1750-3841.2010.01686.x.

[20] R. Davis, Y. Burgula, J. Irudayaraj, B.L. Reuhs, L.J. Mauer, Fourier Transform Infrared (FT-IR) Spectroscopy Coupled with Filtration and Immunomagnetic Separation for the Detection of Escherichia coli O157:H7 in Ground Beef, in: 2010 18th Bienn. Univ. Micro/Nano Symp., IEEE, 2010: pp. 1–6. doi:10.1109/UGIM.2010.5508916.

[21] A. Oust, T. Møretrø, C. Kirschner, J.A. Narvhus, A. Kohler, FT-IR spectroscopy for identification of closely related lactobacilli., J. Microbiol. Methods. 59 (2004) 149–62. doi:10.1016/j.mimet.2004.06.011.

[22] K.M. McCabe, G. Khan, Y.-H. Zhang, E.O. Mason, E.R.B. McCabe, Amplification of Bacterial DNA Using Highly Conserved Sequences: Automated Analysis and Potential for Molecular Triage of Sepsis, Pediatrics. 95 (1995) 165–169.

[23] A. Ulrici, S. Serranti, C. Ferrari, D. Cesare, G. Foca, G. Bonifazi, Efficient chemometric strategies for PET–PLA discrimination in recycling plants using hyperspectral imaging, Chemom. Intell. Lab. Syst. 122 (2013) 31–39. doi:10.1016/j.chemolab.2013.01.001.

[24] S. Prati, M. Quaranta, G. Sciutto, I. Bonacini, L. Litti, M. Meneghetti, et al., Use of nano gold obtained by laser ablation for SEIRA analyses of colorants, Herit. Sci. 2 (2014) 28. doi:10.1186/s40494-014-0028-8.

[25] A. Savitzky, M.J.E. Golay, Smoothing and Differentiation of Data by Simplified Least Squares Procedures, Anal. Chem. 36 (1964) 1627–1639. doi:10.1021/ac60214a047.

[26] R.J. Barnes, M.S. Dhanoa, S.J. Lister, Standard Normal Variate Transformation and De-trending of Near-Infrared Diffuse Reflectance Spectra, Appl. Spectrosc. 43 (1989) 772–777. doi:10.1366/0003702894202201.

[27] J. Burger, P. Geladi, Hyperspectral NIR image regression part I: calibration and correction, J. Chemom. 19 (2005) 355–363. doi:10.1002/cem.938.

[28] C. Ferrari, G. Foca, A. Ulrici, Handling large datasets of hyperspectral images: reducing data size without loss of useful information., Anal. Chim. Acta. 802 (2013) 29–39. doi:10.1016/j.aca.2013.10.009.

[29] A. Antonelli, M. Cocchi, P. Fava, G. Foca, G.C. Franchini, D. Manzini, et al., Automated evaluation of food colour by means of multivariate image analysis coupled to a wavelet-based classification algorithm, Anal. Chim. Acta. 515 (2004) 3–13. doi:10.1016/j.aca.2004.01.005.

[30] G. Foca, F. Masino, A. Antonelli, A. Ulrici, Prediction of compositional and sensory characteristics using RGB digital images and multivariate calibration techniques., Anal. Chim. Acta. 706 (2011) 238–45. doi:10.1016/j.aca.2011.08.046.

[31] A. Ulrici, G. Foca, M.C. Ielo, L.A. Volpelli, D. Pietro Lo Fiego, Automated identification and visualization of food defects using RGB imaging: Application to the detection of red skin defect of raw hams, Innov. Food Sci. Emerg. Technol. 16 (2012) 417–426. doi:10.1016/j.ifset.2012.09.008.

[32] M. Khanmohammadi, S. Armenta, S. Garrigues, M. de la Guardia, Mid- and near-infrared determination of metribuzin in agrochemicals, Vib. Spectrosc. 46 (2008) 82–88.

doi:10.1016/j.vibspec.2007.10.005.

[33] F. Cámara-Martos, G. Zurera-Cosano, R. Moreno-Rojas, R.M. García-Gimeno, F. Pérez-Rodríguez, Identification and Quantification of Lactic Acid Bacteria in a Water-Based Matrix with Near-Infrared Spectroscopy and Multivariate Regression Modeling, Food Anal. Methods. 5 (2011) 19–28. doi:10.1007/s12161-011-9221-5.

[34] F.J.G. Schreurs, Post-mortem changes in chicken muscle, Worlds. Poult. Sci. J. 56 (2000) 319–346. doi:10.1079/WPS20000023.

[35] M. Lin, M. Al-Holy, M. Mousavi-Hesary, H. Al-Qadiri, A.G. Cavinato, B.A. Rasco, Rapid and quantitative detection of the microbial spoilage in chicken meat by diffuse reflectance spectroscopy (600-1100 nm)., Lett. Appl. Microbiol. 39 (2004) 148–55. doi:10.1111/j.1472-765X.2004.01546.x.

[36] H.-J. He, D.-W. Sun, D. Wu, Rapid and real-time prediction of lactic acid bacteria (LAB) in farmed salmon flesh using near-infrared (NIR) hyperspectral imaging combined with chemometric analysis, Food Res. Int. 62 (2014) 476–483. doi:10.1016/j.foodres.2014.03.064.

[37] F. Tao, Y. Peng, C.L. Gomes, K. Chao, J. Qin, A comparative study for improving prediction of total viable count in beef based on hyperspectral scattering characteristics, J. Food Eng. 162 (2015) 38–47. doi:10.1016/j.jfoodeng.2015.04.008.

[38] D.F. Barbin, G. ElMasry, D.-W. Sun, P. Allen, N. Morsy, Non-destructive assessment of microbial contamination in porcine meat using NIR hyperspectral imaging, Innov. Food Sci. Emerg. Technol. 17 (2013) 180–191. doi:10.1016/j.ifset.2012.11.001.

[39] A. Alvarez-Ordóñez, D.J.M. Mouwen, M. López, M. Prieto, Fourier transform infrared spectroscopy as a tool to characterize molecular composition and stress response in foodborne pathogenic bacteria., J. Microbiol. Methods. 84 (2011) 369–78. doi:10.1016/j.mimet.2011.01.009.

[40] J. Samelis, E. Tsakalidou, J. Metaxopoulos, G. Kalantzopoulos, Differentiation of Lactobacillus sake and Lact. curvatus isolated from naturally fermented Greek dry salami by SDS-PAGE of whole-cell proteins, J. Appl. Bacteriol. 78 (1995) 157–163. doi:10.1111/j.1365-2672.1995.tb02836.x.

[41] M.J. Benito, M.J. Serradilla, S. Ruiz-Moyano, A. Martín, F. Pérez-Nevado, M.G. Córdoba, Rapid differentiation of lactic acid bacteria from autochthonous fermentation of Iberian dry-fermented sausages., Meat Sci. 80 (2008) 656–61. doi:10.1016/j.meatsci.2008.03.002.

[42] C. Ferrari, G. Foca, R. Calvini, A. Ulrici, Fast exploration and classification of large hyperspectral image datasets for early bruise detection on apples, Chemom. Intell. Lab. Syst. 146 (2015) 108–119. doi:10.1016/j.chemolab.2015.05.016.

Figure Captions

Figure 1. Profiles of the average hyperspectrograms obtained for the three classes.

Figure 2. Scores plots obtained for the E (a) and the G (b) series. White symbols for gel samples, red for *L. curvatus* and blue for *L. sakei*; triangles and circles distinguish the analysis sessions.

Figure 3. Average intensity gray-scale image of a *L. curvatus* sample before (a) and after (b) segmentation.

Figure 4. Scores plot obtained from PCA applied to the Petri dishes hyperspectrograms dataset. White symbols identify gel samples, red *L. curvatus* and blue *L. sakei*. Different symbols indicate different measurement replicates on the same samples.

Figure 5. PC1-PC3 score (a) and loading (b) plots of FT-MIR RAS spectra recorded for *L. curvatus* (red scores) and *L sakei* (blue scores) on agar gel.

Figure 6. PC1-PC2 score (a) and loading (b) plots of FT-MIR reflection spectra recorded for cooked ham (green scores), and cooked ham artificially contaminated with *L. curvatus* (red scores) and *L sakei* (blue scores), respectively.

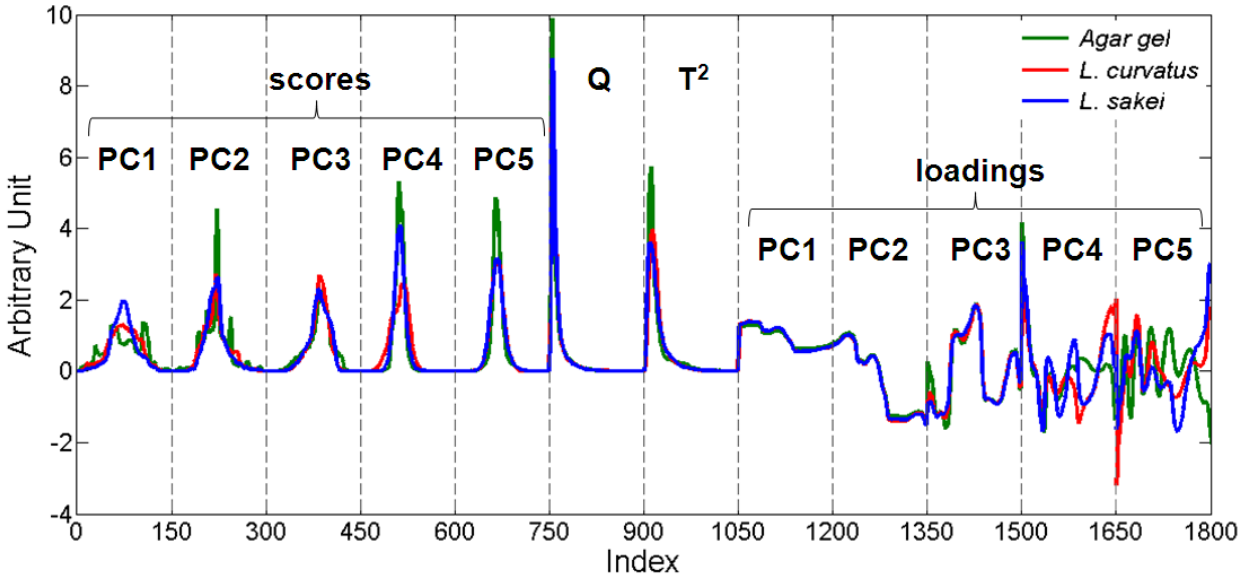
scores
Q
T²
loadings
PC1
PC2
PC3
PC4
PC5
PC1
PC2
PC3
PC4
PC5
Agar gel
L. curvatus
L. sakei
Arbitrary Unit
Index
10
8
6
4
2
0
-2
-4
0
150
300
450
600
750
900
1050
1200
1350
1500
1650
1800

Figure 1

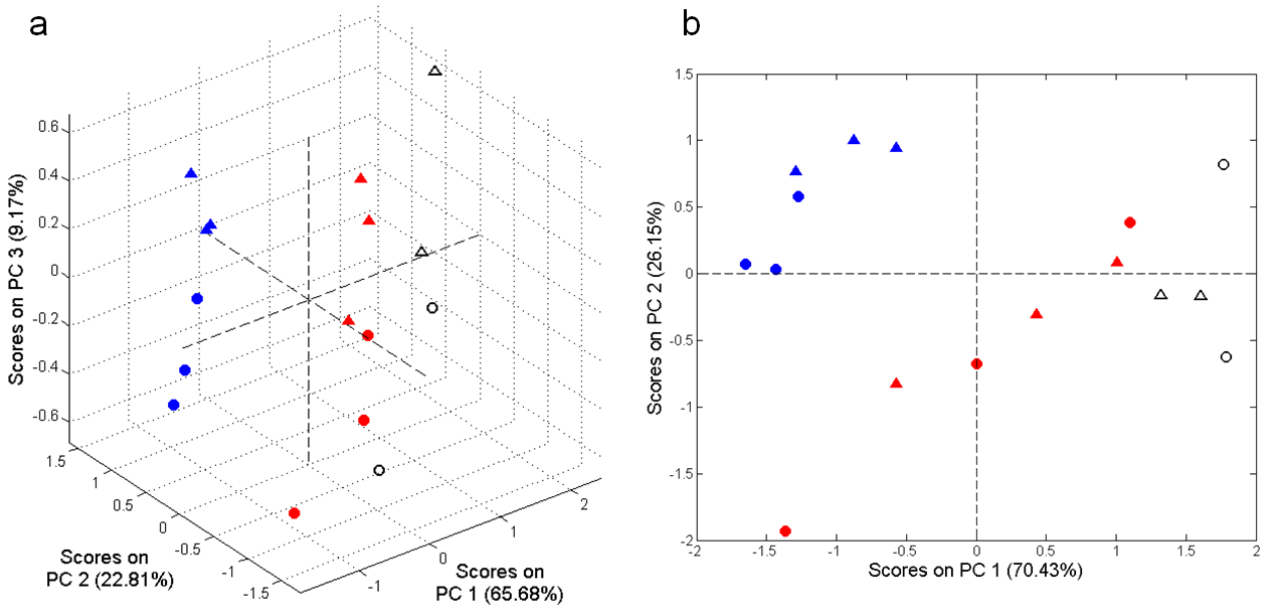

661

662

663 Figure 2

664

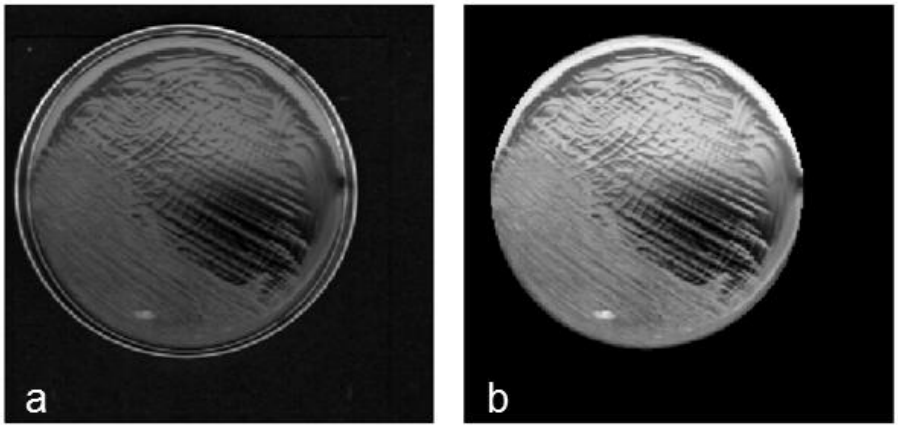

Figure 3

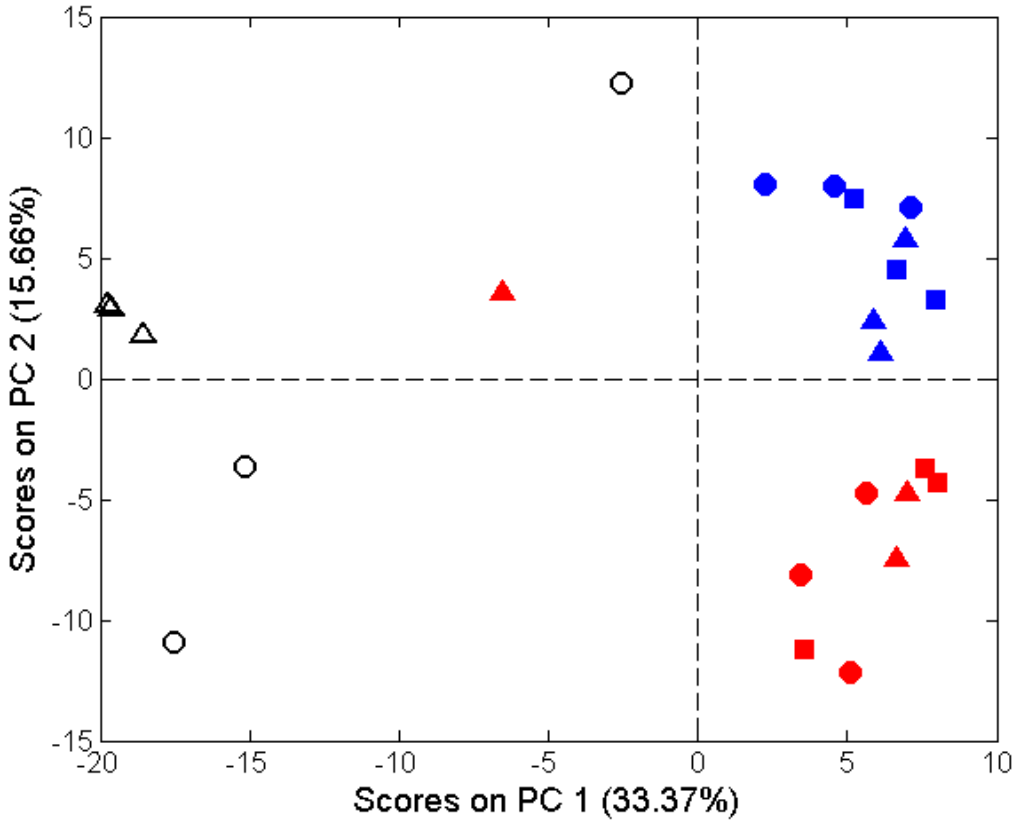

669

670

671 Figure 4

672

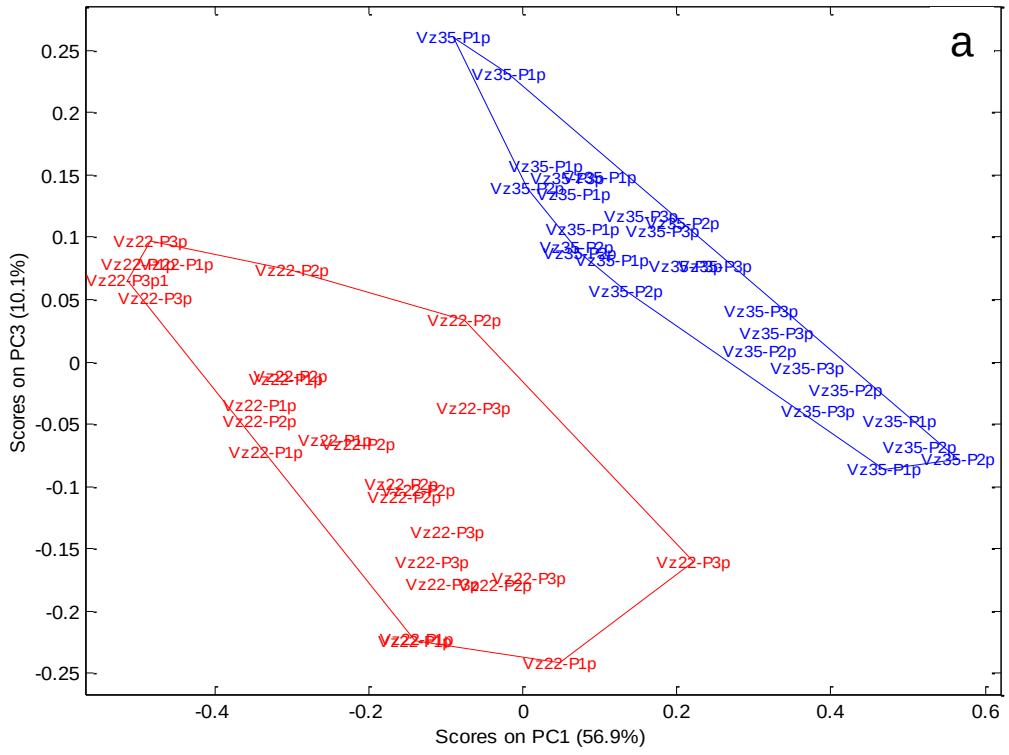

673

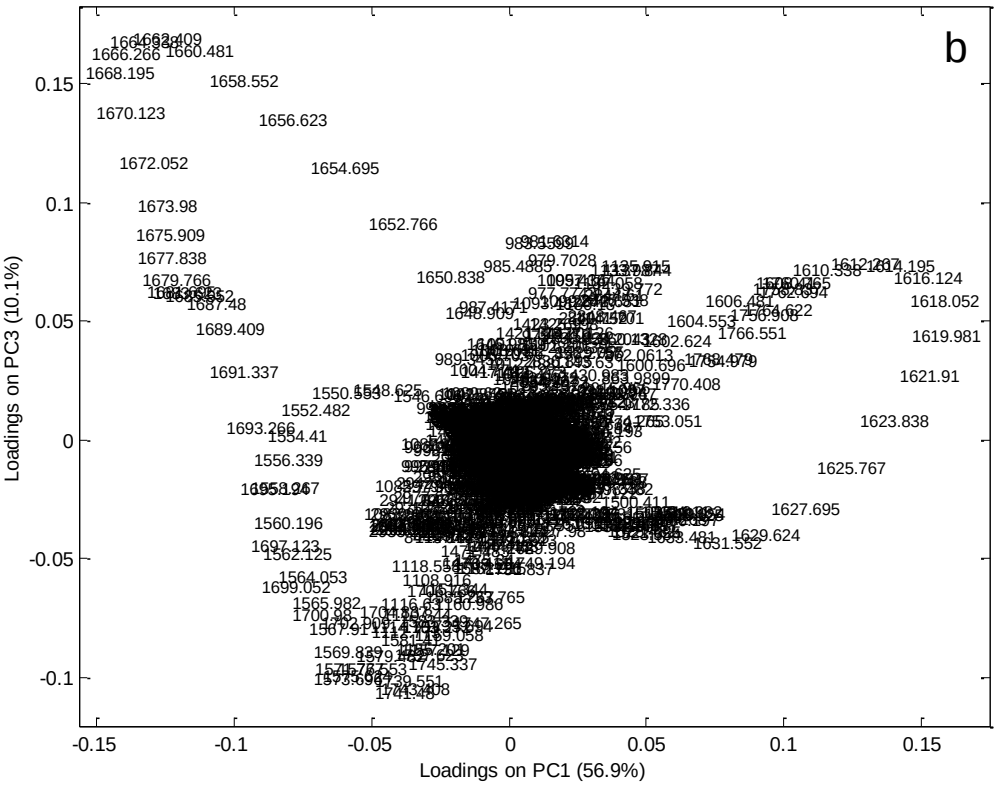

674

675

676 Figure 5

677

678

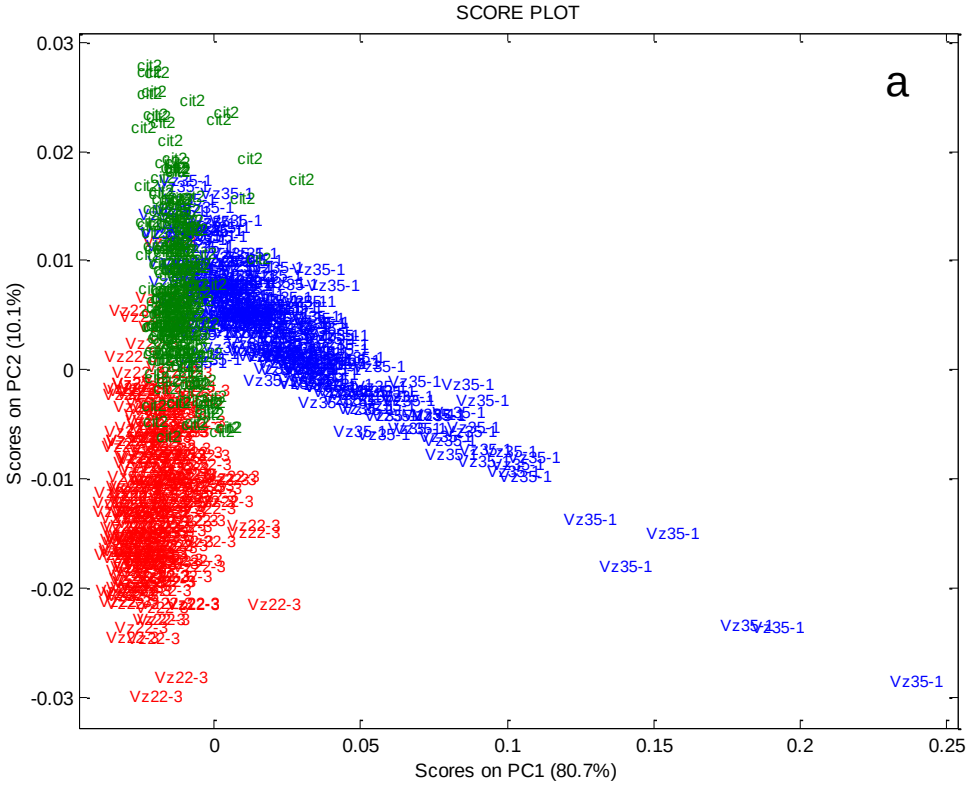

679

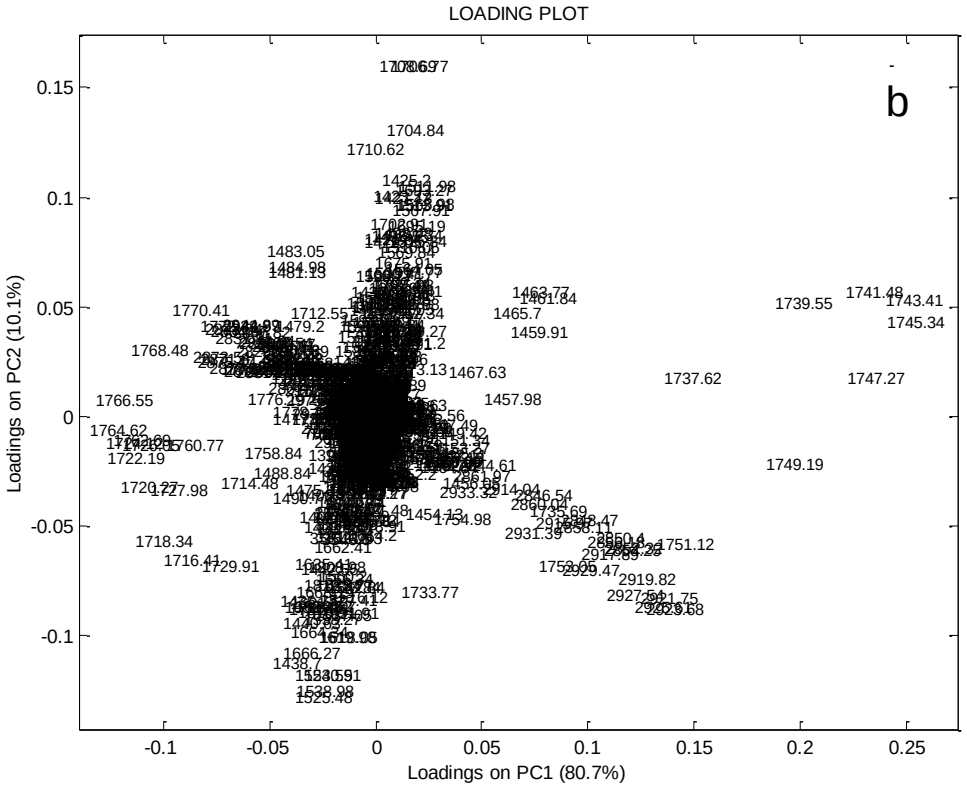

680

681 Figure 6

682